Nonlinear Dyn (2008) 52: 27–34
DOI 10.1007/s11071-007-9253-y

ORIGINAL PAPER

Isolated large amplitude periodic motions of towed rigid wheels

Dénes Takács · Gábor Stépán · S. John Hogan

Received: 8 August 2006 / Accepted: 19 February 2007 / Published online: 26 April 2007

Abstract This study investigates a low degree-of-freedom (DoF) mechanical model of shimmying wheels. The model is studied using bifurcation theory and numerical continuation. Self-excited vibrations, that is, stable and unstable periodic motions of the wheel, are detected with the help of Hopf bifurcation calculations. These oscillations are then followed over a large parameter range for different damping values by means of the software package AUTO97. For certain parameter regions, the branches representing large-amplitude stable and unstable periodic motions become isolated following an isola birth. These regions are extremely dangerous from an engineering point of view if they are not identified and avoided at the design stage.

Keywords Wheel · Shimmy · Bifurcation · Continuation · Stability

Research Group on Dynamics of Machines and Vehicles, Hungarian Academy of Sciences.

D. Takács (✉) · G. Stépán
Department of Applied Mechanics, Budapest University of Technology and Economics, Budapest, Hungary
e-mail: takacs@mm.bme.hu

S.J. Hogan
Department of Engineering Mathematics, University of Bristol, Bristol, UK

1 Introduction

Shimmy is a common name for the lateral vibration of a towed wheel. This has been a well-known phenomenon in vehicle systems dynamics for several decades: the name shimmy comes from a dance that was popular in the 1930s. One of the early scientific studies of shimmy dates back to this time (see [1]). In many cases, the appearance of shimmy is a serious problem, for example, in case of nose gears of airplanes or front wheels of motorcycles. There are many mechanical models (see, for example, [2–7]) that describe the shimmy of rolling wheels. The two most important considerations of any model involve whether the wheel is rigid or elastic and whether the suspension system is rigid or elastic. The simplest combination of a rigid wheel and a rigid suspension system does not, by definition, support lateral vibrations. Lateral vibration can occur in models with an elastic wheel and a rigid suspension (see [8]) and in models where both the wheel and the suspension system are elastic. But in this paper we wish to make analytic progress in order to obtain a clear understanding of the dynamics and so we consider a low degree of freedom (DoF) mechanical model of a rigid wheel, which has a viscously damped elastic suspension. This model was studied without damping in [9], where subcritical Hopf bifurcations and chaotic and transient chaotic oscillations were found.

This paper is structured as follows. First, in Sect. 2, the mechanical model is introduced, together with the

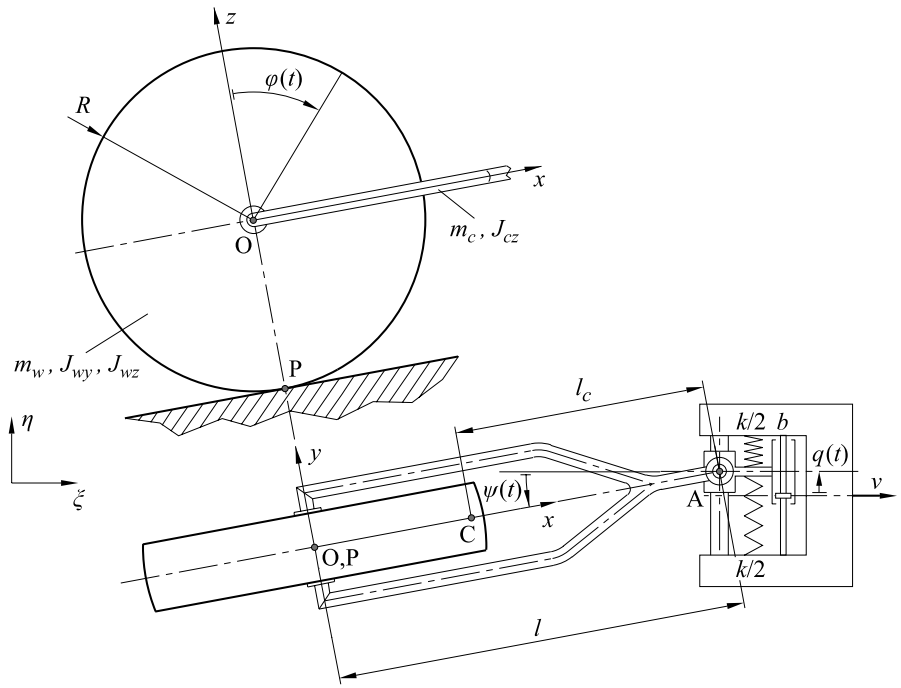

Fig. 1 Model of rigid wheel

equations of motion. In Sects. 3 and 4, the Hopf bifurcation calculation is presented in the presence of viscous damping at the suspension. The effect of damping on the stability of stationary rolling is analysed. In Sect. 5, the periodic solutions of the system are followed using AUTO97 [10], the stability charts and the bifurcation diagrams are plotted and also compared to available analytical results.

The bifurcation diagrams show an isola birth where isolated large amplitude stable and unstable periodic motions coexist with the stable stationary rolling solution. These motions are difficult to detect either by numerical simulation or by conventional stability and bifurcation analysis. The presence of unstable periodic motions indicates a dangerous system configuration.

2 Mechanical model

The mechanical model under consideration is shown in Fig. 1. The plane of the rigid wheel is always vertical to the ground, contacting at a single point P. The radius of the wheel is R, the mass of the wheel is m_w and its mass moment of inertia with respect to the z axis is J_{wz}. The mass moment of inertia with respect to the y axis of its rotation is J_{wy}, where the subscript w refers to the wheel. The caster length is l, and the distance between the center of gravity C of the caster and the king pin at A is l_c. The mass of the caster is m_c and the mass moment of inertia with respect to the z axis at C is J_{cz}, with the subscript c referring to the caster. The system is towed in the horizontal plane with constant velocity v. The king pin is supported by lateral springs of overall stiffness k and viscous damping coefficient b.

Without rolling constraints, the system has 3 degrees of freedom, so one can choose the caster angle ψ, the king pin lateral position q, and the wheel rotation angle φ as general coordinates. The constraint of rolling (without sliding) means that the contact point P has zero velocity. This rolling condition leads to two scalar kinematical constraint equations in the form of coupled first order nonlinear ordinary differential equations (ODEs) with respect to the general coordinates.

The equations of motion of this rheonomic and nonholonomic system can be derived with the help of the Routh–Voss equations or the Appell–Gibbs equations [11]. In the case of zero damping ($b = 0$), they are given in [12]. Here, we present the equations for nonzero viscous damping:

$$\begin{aligned}
\dot{\psi} &= \vartheta,\\
\dot{\vartheta} &= -\frac{N(\psi,\vartheta,q)}{D(\psi)},\\
\dot{q} &= v\tan\psi + \frac{l}{\cos\psi}\vartheta,\\
\dot{\varphi} &= \frac{v + l\dot{\psi}\sin\psi}{R\cos\psi},
\end{aligned} \tag{1}$$

where

$$\begin{aligned}
&N(\psi,\vartheta,q)\\
&\quad= \left(-(m_w l + m_c l_c)v + \frac{lv}{R^2}J_{wy}\tan^2\psi\right.\\
&\qquad\left. + \frac{(m_w+m_c)lv}{\cos^2\psi} + \frac{bl^2}{\cos\psi}\right)\vartheta\\
&\qquad + \left((m_w+m_c)l^2 + \frac{l^2}{R^2}J_{wy}\right)\frac{\sin\psi}{\cos^2\psi}\vartheta^2\\
&\qquad + klq + blv\tan\psi
\end{aligned} \tag{2}$$

and

$$\begin{aligned}
D(\psi) &= \left(m_c l_c(l_c - 2l) - m_w l^2 + J_{wz} + J_{cz}\right)\cos\psi\\
&\quad + \left(\frac{(m_w+m_c)l^2}{\cos^2\psi} + \frac{l^2}{R^2}J_{wy}\tan^2\psi\right)\cos\psi
\end{aligned} \tag{3}$$

are odd and even functions respectively of the general coordinates. The first two equations in (1) are the equations of angular momentum and the last two express the constraint of rolling (without sliding) of P.

Since the general coordinate φ appears only in the fourth equation of motion, it is a so-called cyclic coordinate and the system can be described uniquely in the three dimensional phase space of the caster angle ψ, caster angular velocity ϑ and the king pin lateral displacement q.

3 Stability analysis

The trivial solution of the system is stationary rolling along a straight line defined by the vector of the towing velocity:

$$\psi \equiv 0, \qquad \dot{\psi} \equiv 0, \qquad q \equiv 0, \qquad \dot{\varphi} \equiv \frac{v}{R}.$$

When the towing speed is zero, the system forms a 1 DoF oscillator about the z axis at P. The corresponding angular natural frequency ω_n of the undamped linear system and the damping ratio ζ are given by

$$\omega_n = \sqrt{\frac{kl^2}{J_{wz} + J_{cz} + m_c(l-l_c)^2}}, \qquad \zeta = \frac{1}{2}\frac{b}{k}\omega_n. \tag{4}$$

Let us introduce the new dimensionless parameters:

$$L = \frac{l}{l_c}, \qquad V = \frac{v}{\omega_n l_c}, \tag{5}$$

$$\begin{aligned}
\kappa &= \frac{m_c l_c(l-l_c)}{J_{wz} + J_{cz} + m_c(l-l_c)^2},\\
\chi &= \frac{(m_c+m_w)l^2 + J_{wy}l^2/R^2}{J_{wz} + J_{cz} + m_c(l-l_c)^2},
\end{aligned} \tag{6}$$

where L and V are the dimensionless caster length and towing speed respectively, and κ and χ are dimensionless mass moment of inertia parameters related to the caster and wheel geometry and inertia.

With these new parameters, the third-order Taylor series expansion of the first three governing equations (1) about the trivial solution assumes the form:

$$\begin{aligned}
&\begin{bmatrix} \dot{\psi}\\ \dot{\vartheta}\\ \dot{q}/l_c \end{bmatrix}\\
&= \begin{bmatrix} 0 & 1 & 0\\ -2\zeta V{\omega_n}^2/L & -\omega_n(2\zeta+\kappa V) & -{\omega_n}^2/L\\ \omega_n V & L & 0 \end{bmatrix}\begin{bmatrix} \psi\\ \vartheta\\ q/l_c \end{bmatrix}\\
&\quad + \begin{bmatrix} 0\\ -\omega_n\left((2\zeta+\kappa V)(1-\chi) + V\left(\frac{\chi}{L} - \frac{\kappa}{2}\right)\right)\psi^2\vartheta\\ \frac{\omega_n V}{3}\psi^3 + \frac{L}{2}\psi^2\vartheta \end{bmatrix}\\
&\quad + \begin{bmatrix} 0\\ -\chi\psi\vartheta^2 - \frac{{\omega_n}^2}{L}\left(\frac{1}{2}-\chi\right)\psi^2\frac{q}{l_c} - \frac{2\zeta V{\omega_n}^2}{L}\left(\frac{5}{6}-\chi\right)\psi^3\\ 0 \end{bmatrix}.
\end{aligned} \tag{7}$$

The characteristic equation is obtained from the linear coefficient matrix of (7):

$$\begin{aligned}
&\lambda^3 + (2\zeta+\kappa V)\omega_n\lambda^2 + \left(1 + \frac{2\zeta V}{L}\right){\omega_n}^2\lambda\\
&\quad + \frac{V}{L}{\omega_n}^3 = 0.
\end{aligned} \tag{8}$$

According to the Routh–Hurwitz criterion, the stability of the stationary rolling is equivalent to:

$$L \geq L_{\mathrm{cr}}(V) = \frac{V(1 - 4\zeta^2 - 2\zeta\kappa V)}{2\zeta + \kappa V}, \tag{9}$$

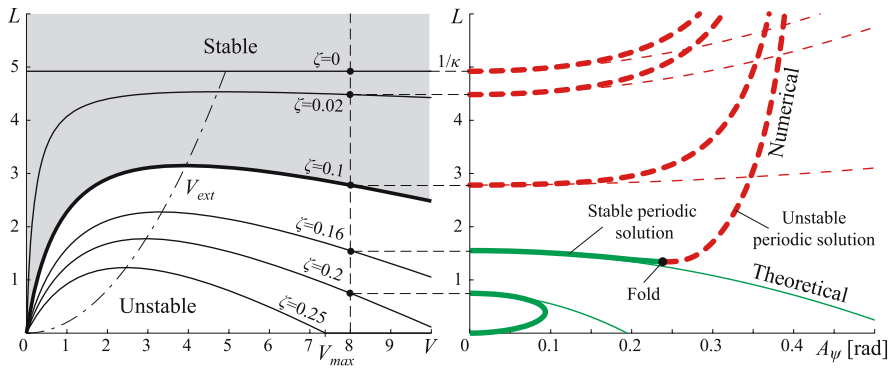

a. The linear stability chart b. Bifurcation branches

Fig. 2 The stability chart and the bifurcation branches of the dimensionless system

considering positive parameter values only. At fixed damping ratios ζ, the stability boundary curves are characterized by

$$V_{\text{ext}} = \frac{1-2\zeta}{\kappa}, \qquad V_{\max} = \frac{1-4\zeta^2}{2\zeta\kappa}, \tag{10}$$

where $\mathrm{d}L_{\text{cr}}(V)/\mathrm{d}V = 0$ at $V = V_{\text{ext}}$ and $L_{\text{cr}}(V) = 0$ at $V = V_{\max}$. Stationary rolling is always stable for $V > V_{\max}$ or $L > L_{\text{cr}}(V_{\text{ext}})$. Figure 2(a) shows the corresponding stability chart in the plane of the dimensionless towing speed V and caster length L for $\kappa = 0.203$ and $\chi = 5.67$. The stability region is shaded for $\zeta = 0.1$. The dot-dash line is the locus of V_{ext} as a function of ζ. Our parameters come from a realistic towed wheel of a shopping trolley. The parameters of the wheel are $m_w = 0.3519$ [kg], $J_{wy} = 4.63 \times 10^{-5}$ [kg m^2], $J_{wz} = 2.38 \times 10^{-5}$ [kg m^2] and $R = 0.04$ [m]. The data of the caster are $m_c = 0.0668$ [kg], $l_c = 0.012$ [m] and $J_{cz} = 3.48 \times 10^{-6}$ [kg m^2]. We shall discuss Fig. 2(b) in Sect. 4.

The stability chart in dimensional terms is of course of great practical use to engineers. However the natural choice of scaling in (5) makes it difficult to immediately deduce its form from Fig. 2(a). Hence we redraw this figure in dimensional terms in Fig. 3, using the shopping trolley parameters.

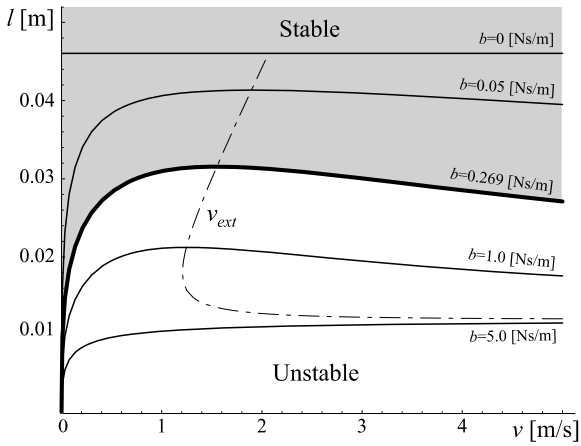

Fig. 3 Stability boundaries of the linear system in dimensional form using the shopping trolley parameters

4 Hopf bifurcation

Despite giving a more useful stability chart, the dimensional form is less amenable to analysis. In dimensionless form the stability calculations are simpler and clearer.

The eigenvalues of the linear coefficient matrix of the dimensionless system can be determined on the stability boundary when $L = L_{\text{cr}}$ as given in (9). There are two complex conjugate eigenvalues with zero real part and one negative real eigenvalue:

$$\lambda_{1,2} = \pm i\omega, \qquad \lambda_3 = -\omega_n(2\zeta + \kappa V), \tag{11}$$

where

$$\omega = \frac{\omega_n}{\sqrt{1-4\zeta^2-2\zeta\kappa V}}, \tag{12}$$

hence, there is Hopf bifurcation on the stability boundary. The eigenvectors $\{\mathbf{s}_1, \mathbf{s}_2, \mathbf{s}_3\}$ can also be determined:

$$\mathbf{s}_1 = \bar{\mathbf{s}}_2 = \begin{bmatrix} \omega^2(2\zeta+\kappa V)(1+\mathrm{i}\frac{\omega}{\omega_n}(2\zeta+\kappa V)) \\ -\omega^3(2\zeta+\kappa V)(\frac{\omega}{\omega_n}(2\zeta+\kappa V)-\mathrm{i}) \\ V({\omega_n}^2+\omega^2(2\zeta+\kappa V)^2) \end{bmatrix}, \quad \mathbf{s}_3 = \begin{bmatrix} -1 \\ \omega_n(2\zeta+\kappa V) \\ 2\zeta V \end{bmatrix}. \tag{13}$$

The transformation matrix $\mathbf{T}$ can be constructed from the eigenvectors in the following way:

$$\mathbf{T} = [\mathrm{Re}\,\mathbf{s}_1 \;\; \mathrm{Im}\,\mathbf{s}_1 \;\; \mathbf{s}_3]. \tag{14}$$

Let us introduce new variables $[x_1, x_2, x_3]$ such that:

$$\begin{bmatrix} \psi \\ \vartheta \\ q/l_c \end{bmatrix} = \mathbf{T} \begin{bmatrix} x_1 \\ x_2 \\ x_3 \end{bmatrix}. \tag{15}$$

If we substitute this into (7) and we multiply the equation on the left with the inverse of the transformation matrix, the Poincaré normal form is calculated, which has the form

$$\begin{bmatrix} \dot{x}_1 \\ \dot{x}_2 \\ \dot{x}_3 \end{bmatrix} = \begin{bmatrix} 0 & \omega & 0 \\ -\omega & 0 & 0 \\ 0 & 0 & -(2\zeta+\kappa V)\omega \end{bmatrix} \begin{bmatrix} x_1 \\ x_2 \\ x_3 \end{bmatrix} + \begin{bmatrix} \sum_{\substack{j+k=3 \\ j,k>0}} a_{jk} x_1^j x_2^k + \cdots \\ \sum_{\substack{j+k=3 \\ j,k>0}} b_{jk} x_1^j x_2^k + \cdots \\ \cdots \end{bmatrix}. \tag{16}$$

Since the nonlinearities are symmetric (i.e., there are no second degree terms in the nonlinear part of the Poincaré normal form), the centre manifold is approximated by a second degree surface. Thus, the transformation of the nonlinear part needs only the terms in x_1 and x_2. The terms in which x_3 appear can be neglected. The sense of the Hopf bifurcation comes from the reduced form of Poincaré–Lyapunov parameter δ for the symmetric case (see [13]):

$$\delta = \frac{1}{8}(3a_{30} + a_{12} + b_{21} + 3b_{03}), \tag{17}$$

so

$$\delta = \frac{\omega_n(2\zeta+\kappa V)^2}{8V^2} \times \frac{\zeta+\kappa V-(2\zeta+\kappa V)\frac{\omega^2}{\omega_n^2}(2-\zeta\kappa V+\chi(\frac{\omega^2}{\omega_n^2}-2))}{(1+(2\zeta+\kappa V)^2\frac{\omega_n^2}{\omega^2})((2\zeta+\kappa V)^2+\frac{\omega_n^2}{\omega^2})}. \tag{18}$$

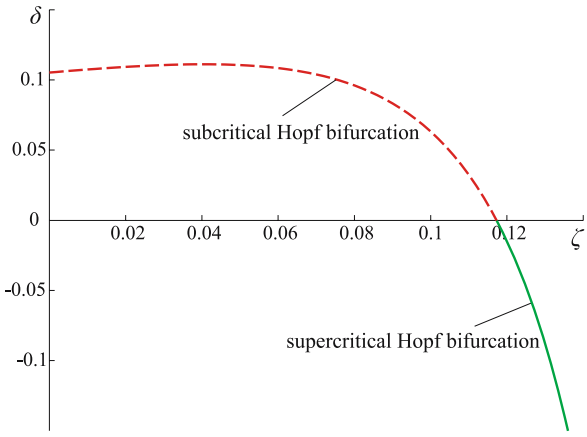

Fig. 4 The δ parameter in (18) as a function of the damping ζ

If δ is positive/negative then the periodic orbit of the Hopf bifurcation is subcritical/supercritical, namely unstable/stable. If we set $V = 8$ and take $\kappa = 0.203$ and $\chi = 5.67$ as before, δ can be plotted as a function of the damping ζ, see Fig. 4. In our case the sign of δ changes at a critical value of the damping.

To compare our results with numerical continuation, the theoretical bifurcation branch has to be calculated. Accordingly the real part of the implicit derivative of the characteristic equation with respect to the bifurcation parameter L has to be determined at the critical parameter value L_{cr}:

$$\mathrm{Re}\left.\frac{\mathrm{d}\lambda}{\mathrm{d}L}\right|_{L=L_{\mathrm{cr}}} = -\frac{\omega_n(2\zeta+\kappa V)^2}{2V(1+(2\zeta+\kappa V)^2\frac{\omega_n^2}{\omega^2})}. \tag{19}$$

The amplitude of the periodic orbit is given by

$$r = \sqrt{-\frac{\mathrm{Re}\,\lambda'|_{L=L_{\mathrm{cr}}}}{\delta}(L-L_{\mathrm{cr}})}, \tag{20}$$

namely

$$r = \sqrt{\frac{4V((2\zeta+\kappa V)^2+\frac{\omega_n^2}{\omega^2})}{\zeta+\kappa V-(2\zeta+\kappa V)\frac{\omega^2}{\omega_n^2}(2-\zeta\kappa V+\chi(\frac{\omega^2}{\omega_n^2}-2))}(L-L_{\mathrm{cr}})}. \tag{21}$$

With the help of the transformation matrix $\mathbf{T}$, the amplitude of the vibration can be plotted with respect to the general coordinates ψ, ϑ and q. The theoretical branches of the amplitude of ψ (A_ψ) are compared with the numerically continued results of the dimensionless system (7) in Fig. 2(b). In this figure, as in the remainder of the paper, dashed lines mean unstable

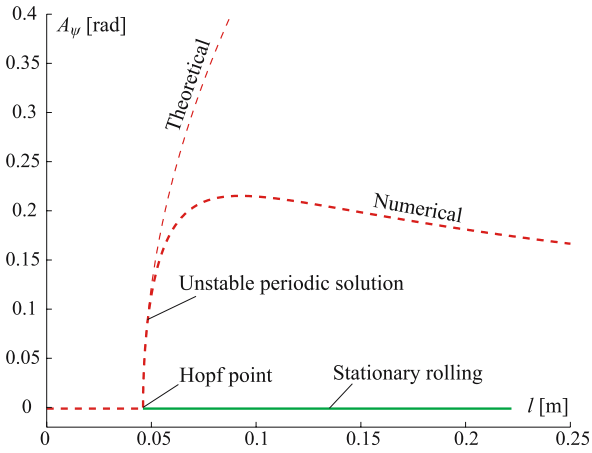

Fig. 5 The theoretical and numerical bifurcation branches of the undamped system

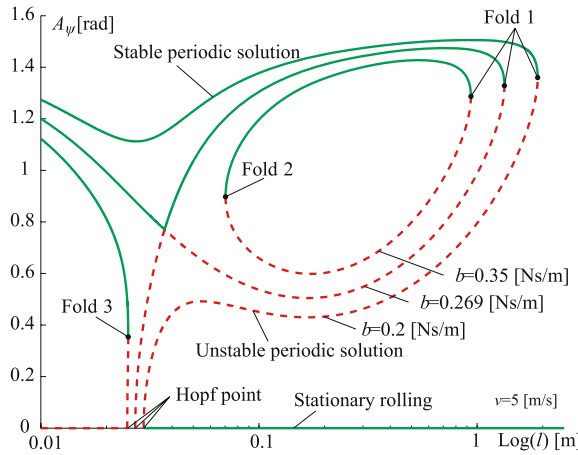

Fig. 6 Bifurcation diagrams of the damped system with the isola birth

branches and continuous lines mean stable solutions, and thick and thin lines show numerical and theoretical results, respectively. When the bifurcations are supercritical, the numerical continuation shows the existence of folds in certain parameter regions, leading to large amplitude unstable periodic motions.

As mentioned at the start of this section, the analysis of the damped dimensional system is difficult. But in the case of zero damping the sense of the Hopf bifurcation, the Poincaré–Lyapunov parameter δ, can be determined:

$$\delta = \frac{v\omega^4 l}{8m_c(l-l_c)(v^2+\omega^2 l^2)^2} \times \left(m_w l + m_c l_c + \frac{l}{R^2} J_{wy}\right) > 0, \qquad (22)$$

which is always positive for all real parameter values, namely the Hopf bifurcation is always subcritical (i.e., the periodic orbit is always unstable). The comparison of the theoretical and numerical results is shown in Fig. 5.

5 Numerical continuation

Returning now to the damped case (with $b = 0.2$ [Ns/m]), the branch of unstable periodic solutions was followed using AUTO97 [10] from the Hopf point and a saddle-node bifurcation (fold) was detected, as in Fig. 6. This means that the damped system also has stable periodic solutions. So if the system is perturbed

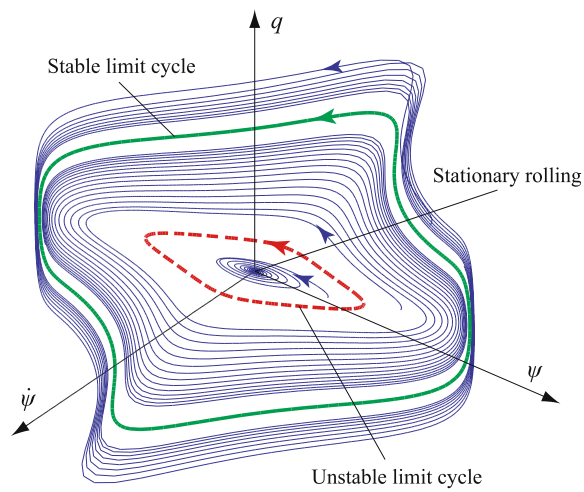

Fig. 7 The trajectories in the phase space for $b = 0.269$ [Ns/m]

enough then it will be attracted to these large amplitude stable periodic solutions.

If the damping factor is increased, the peaks of the stable and unstable branches move closer together. At a critical damping factor ($b = 0.269$ [Ns/m]) the branches intersect each other and an isola is born, shown in Fig. 6. Simulated motions are shown in phase space in Fig. 7. So a separated periodic solution branch occurs in the bifurcation diagram for $b >$ 0.269 [Ns/m]. There are now three folds in the figure and, by changing the damping factor b or the towing velocity v, the location of these folds also changes.

In practice such large amplitude stable periodic motions might be expected to slide, once a certain crit-

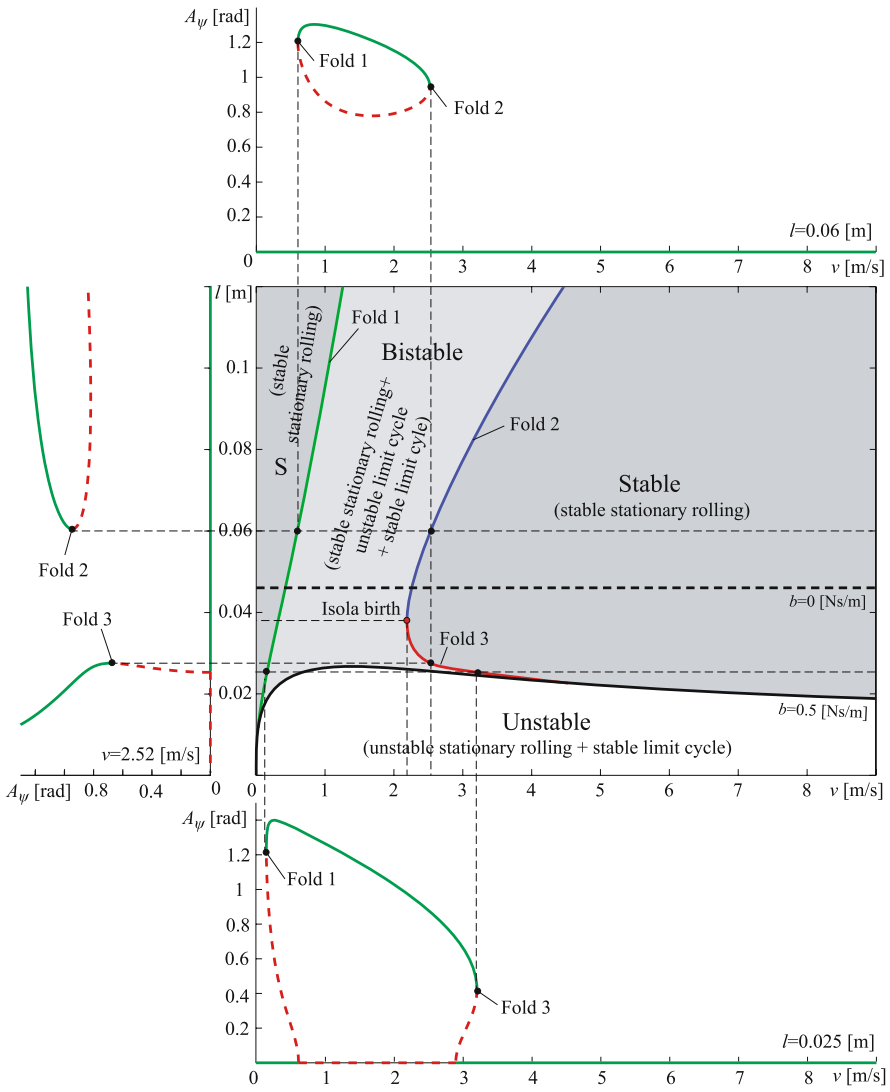

Fig. 8 Stability chart of the nonlinear system

ical friction force is reached. Although we consider rolling, slipping is not part of our model and this would have to be included if we wished to be certain that such motions could be observed in practice.

For fixed damping ratio a nonlinear stability chart can be plotted in the (v, l) plane, where the location of the folds can also be marked. With different projections, the nonlinear behavior of the system is represented in Fig. 8.

The bistable area is of great importance. It has been found only with numerical continuation. That means that the very dangerous large amplitude periodic motion cannot be discovered analytically in this case. This bistable area can be reduced and bounded for large enough damping ratio. This is shown in Fig. 9.

6 Conclusions

The importance in the investigation of the assumption of a rigid wheel model can be questioned, because a real system is more complex. However, the point of our study is to show that the well-known properties of shimmy, for example the existence of unstable large amplitude periodic motions, are present even in this simple model.

In this paper the damped model was considered using analytical and numerical methods. It was shown that the subcritical Hopf bifurcation can change to supercritical if the damping ratio is increased. In the damped system a separated branch of periodic large amplitude solutions was detected using numerical con-

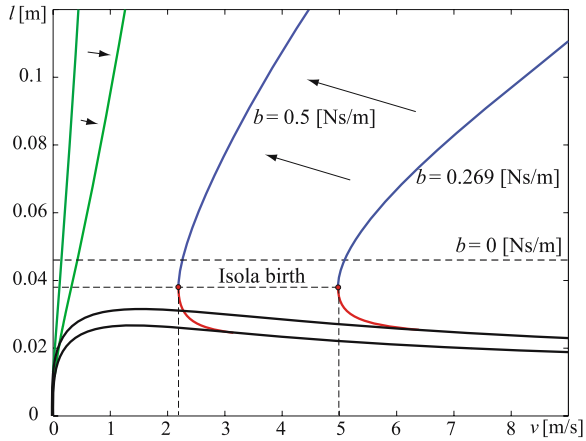

Fig. 9 Stability boundaries at different damping factors

tinuation. For some parameter values, the stationary rolling solution is stable for any value of the towing speed, but there is also a separated periodic solution branch, a so-called isola of large amplitude, which is very dangerous. This region cannot be determined by linear analysis. Therefore, without the nonlinear numerical investigation a system may be designed with parameter values that allow for the presence of these dangerous solutions.

Acknowledgements The authors greatly acknowledge the financial support provided by the Hungarian National Science Foundation under grant No. T043368.

References

1. Schlippe, B.V., Dietrich, R.: Shimmying of pneumatic wheel. Lilienthal-Gesellschaft für Luftfahrtforschung, Bericht **140**, 125–160 (1941) translated for the AAF in 1947 by Meyer & Company
2. Pacejka, H.B.: Tyre and Vehicle Dynamics. Elsevier, Amsterdam (2002)
3. Sharp, R.S., Jones, C.J.: A comparison of tyre representations in a simple wheel shimmy problem. Veh. Syst. Dyn. **9**, 45–47 (1980)
4. Plaut, R.H.: Rocking instability of a pulled suitcase with two wheels. Acta Mech. **117**, 165–179 (1996)
5. O'Reilly, O.M., Varadi, P.C.: A traveler's woes: some perspectives from dynamical systems. In: Moon, F.C. (ed.) Applications of Nonlinear and Chaotic Dynamics in Mechanics, pp. 397–406. Kluwer Academic, Dordrecht (1996)
6. Kacani, V., Stribersky, A., Troger, H.: Maneuverability of a truck-trailer combination after loss of lateral stability. Veh. Syst. Dyn. **17**, 186–198 (1988)
7. Le Saux, C., Leine, R.I., Glocker, C.: Dynamics of a rolling disk in the presence of dry friction. J. Nonlinear Sci. **15**(1), 27–61 (2005)
8. Stépán, G.: Delay, nonlinear oscillations and shimmying wheels. In: Moon, F.C. (ed.) Applictions of Nonlinear and Chaotic Dynamics in Mechanics, pp. 373–386. Kluwer Academic, Dordrecht (1999)
9. Stépán, G.: Chaotic motion of wheels. Veh. Syst. Dyn. **20**(6), 341–351 (1991)
10. Doedel, E.J., Champneys, A.R., Fairgrieve, T.F., Kuznetsov, Yu.A., Sandstede, B., Wang, X.: AUTO97: Continuation and bifurcation software for ordinary differential equations (with HomCont). Technical Report, Concordia University (1997)
11. Gantmacher, F.: Lectures in Analytical Mechanics. Mir, Moscow (1970)
12. Stépán, G.: Appel–Gibbs equation for classical wheel shimmy—an energy view. J. Comput. Appl. Mech. **3**(1), 85–92 (2002)
13. Stépán, G.: Retarded Dynamical System. Longman, London (1989)